Tilt grain boundary instabilities in three-dimensional lamellar patterns

Zhi-Feng Huang and Jorge Viñals
McGill Institute for Advanced Materials and Department of Physics, McGill University, Montreal, QC H3A 2T8, Canada
(Received 10 November 2004; published 2 March 2005)

We identify a finite wave-number instability of a 90° tilt grain boundary in three-dimensional lamellar phases which is absent in two-dimensional configurations. Both a stability analysis of the slowly varying amplitude or envelope equation for the boundary, and a direct numerical solution of an order parameter model equation are presented. The instability mode involves two-dimensional perturbations of the planar base boundary, and is suppressed for purely one-dimensional perturbations. We find that both the most unstable wave numbers and their growth rate increase with ϵ, the dimensionless distance away from threshold of the lamellar phase.

DOI: 10.1103/PhysRevE.71.031501 PACS number(s): 83.50.−v, 47.54.+r, 61.25.Hq, 05.45.−a

I. INTRODUCTION

The longest relaxation times in partially ordered structures outside of thermodynamic equilibrium are often determined by existing topological defects. Therefore defect structure, interaction, and motion typically control the evolution toward an equilibrium, spatially ordered state. Prototypical example systems that are the subject of current research include Rayleigh-Bénard convection above onset [1,2], and microphase separation in block copolymers [3]. Whereas the former is an effectively two-dimensional system (fluctuations in the heat transport direction are unimportant near the convective threshold), the latter can involve both two-dimensional systems (thin films) as well as three-dimensional bulk samples. In both cases, a transient macroscopic sample usually consists of differently oriented domains (or grains) of the ordered phase with a large number of defects like grain boundaries, dislocations, and disclinations. In order to understand the evolution of such a polycrystalline state, extensive efforts, both theoretical and experimental, have been devoted to the motion of these topological defects, as well as to the related issue of wave-number adjustment and selection.

Of particular interest is recent research on the dynamics of grain boundaries in roll (Rayleigh-Bénard convection) or lamellar (block copolymer) configurations. Most theoretical studies [4–9] are based on phenomenological order parameter models or on amplitude equations which focus on slowly evolving amplitudes of base patterns close to threshold. In two dimensions, a stationary 90° tilt grain boundary configuration has been found that has the same characteristic wave number (q_0) in both ordered domains on either side of the boundary [4,5]. Even though for an infinite roll (or lamellar) configuration there exists a finite range of possible wave-number values (i.e., the "stability balloon" [1,10,11] in the two-dimensional stability diagram), phase-winding motion [5] yields a wave-number selection mechanism for the grain boundary configuration, leading to a unique value of q_0 for both bulk domains. When the wave numbers on either side of the boundary are different [4], or when both differ from q_0 [5], boundary motion follows. Boundary motion can be further induced by roll curvature [7], or by an externally imposed shear flow [8,9].

Most of the known theoretical or numerical results concern two-dimensional configurations. In this paper, on the other hand, we focus on a three-dimensional configuration that also involves a 90° tilt grain boundary. Contrary to the two-dimensional result, this grain boundary configuration is found to be always unstable. The characteristic wave vector for instability is two-dimensional (purely one-dimensional perturbations are stable), with both wave-number components smaller than that of the base lamellar pattern (q_0), and decreasing as the system approaches the order-disorder threshold. The amplitude equation analysis reveals that the three-dimensional instability is associated with a nonzero imaginary part (or phase) of the complex amplitude which grows in time around the boundary region. This is in contrast with perturbations of the two-dimensional stationary state (with a selected wave number q_0) which can be described by real amplitudes alone [2,4,5]. The results of the asymptotic analysis have been verified by direct numerical solution of the Swift-Hohenberg model of convection, and good agreement is found between the power spectra of boundary perturbations numerically determined and the results of the stability analysis based on the amplitude equations. Given that the model equations are of gradient or potential form, we compute the temporal evolution of the energy following the instability. We show that cross roll coupling terms enhance instability in both two and three dimensions. However, these terms remain sufficiently small in the two-dimensional case and are always canceled by larger, stabilizing terms. In three dimensions, the larger phase space available for perturbation leads to the instability. From these results, we would conclude that 90° tilt grain boundaries should be rarely observed in three-dimensional systems, and even then only as transients. There is some evidence in block copolymers that this is in fact the case [12].

In an effort to find regions of stability, we have investigated a number of configurations involving a range of wave numbers, but we have not found any that ultimately leads to a stationary state, perhaps with a distorted boundary. Therefore we cannot comment at this point on the nonlinear growth and possible saturation of the instability, or on whether unstable motion will eventually lead to boundary annihilation.

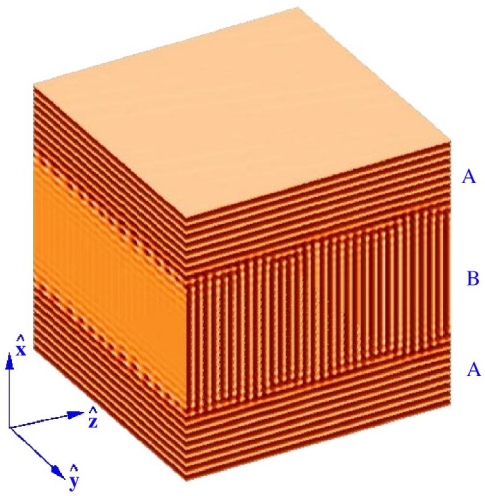

FIG. 1. (Color online) Grain boundary configuration obtained from numerical integration of the Swift-Hohenberg equation (1) in a 256^3 system, for $\epsilon=0.08$, and an initial configuration comprising two symmetric grain boundaries as discussed in the text, plus small random noise uniformly distributed between $(-0.05, 0.05)$. At the time shown ($t=2500$), the instability is readily apparent as undulations along both y and z axes.

Section II describes the geometry of the grain boundary configuration studied, and a weakly nonlinear analysis leading to the stability calculation. The ranges and modes of instability are identified, and the results compared with direct numerical solution of the Swift-Hohenberg model equation. In Sec. III we examine possible instability mechanisms for this case through the comparison between two-dimensional and three-dimensional configurations. Finally, the conclusions following from our results are summarized in Sec. IV.

II. STABILITY ANALYSIS OF A 90° TILT GRAIN BOUNDARY IN THREE DIMENSIONS

Our analysis is based on the Swift-Hohenberg model equation [13], an order parameter equation originally developed to study the convective instability in Rayleigh-Bénard convection, and later used to describe lamellae formation and reorientation in block copolymer melts [14]. In dimensionless units, the equation is

$$\frac{\partial \psi}{\partial t} = \epsilon\psi - (\nabla^2 + q_0^2)^2\psi - \psi^3, \tag{1}$$

where for diblock copolymers the order parameter field ψ represents the local density difference between two constituent monomers, and ϵ is the dimensionless distance from the order-disorder threshold. For $\epsilon>0$ there exists a range of periodic stationary solutions around the wave number q_0 that are linearly stable. In the dimensionless units used $q_0=1$. We retain the symbol q_0 in what follows for the sake of clarity in the presentation.

The system configuration studied here comprises a planar grain boundary separating two perfectly ordered, but differently oriented lamellar domains in three dimensions. We focus on the case of 90° grain boundary, as presented in Fig. 1, for which the lamellar orientations of two domains A and B are perpendicular to each other: $q_A=q_0\hat{x}$ for domain A, and $q_B=q_0\hat{z}$ for domain B. It is well known that in two dimensions (a grain boundary line) [1,4,5] this choice of wave number leads to a stable grain boundary configuration against any small perturbation; however, this is not the case for the three-dimensional (3D) system, as will be shown below.

We introduce a standard multiple scale expansion of Eq. (1) to derive the associated amplitude equations for the 90° tilt grain boundary. The order parameter field ψ is expanded in both regions A and B as the superposition of two base modes e^{iq_0x} and e^{iq_0z},

$$\psi = \frac{1}{\sqrt{3}}(Ae^{iq_0x} + Be^{iq_0z} + \text{c.c.}), \tag{2}$$

with complex amplitudes A and B that are slowly varying in space and time. We set $T=\epsilon t$ for slow time scale, and introduce anisotropic slow spatial scalings, with $X=\epsilon^{1/2}x$, $Y=\epsilon^{1/4}y$, $Z=\epsilon^{1/4}z$ for mode e^{iq_0x}, and $\bar{X}=\epsilon^{1/4}x$, $\bar{Y}=\epsilon^{1/4}y$, $\bar{Z}=\epsilon^{1/2}z$ for mode e^{iq_0z}. Then the governing equations for amplitudes A and B can be obtained [to $O(\epsilon^{3/2})$]

$$\partial_t A = [\epsilon - (2iq_0\partial_x + \partial_y^2 + \partial_z^2)^2]A - |A|^2A - 2|B|^2A, \tag{3}$$

$$\partial_t B = [\epsilon - (\partial_x^2 + \partial_y^2 + 2iq_0\partial_z)^2]B - |B|^2B - 2|A|^2B, \tag{4}$$

where we have reintroduced the original spatial and temporal variables. We note that the only difference with the amplitude equations for a two-dimensional system as given in Ref. [5] is the extra term proportional to ∂_y^2 in each equation, a term which is trivially due to the additional spatial direction available in three-dimensional space.

We first construct a base state solution involving a stationary and planar grain boundary. Since the boundary lies on the yz plane, the amplitudes are only a function of the normal coordinate x:

$$\epsilon A_0 + 4q_0^2\partial_x^2 A_0 - |A_0|^2A_0 - 2|B_0|^2A_0 = 0, \tag{5}$$

$$\epsilon B_0 - \partial_x^4 B_0 - |B_0|^2B_0 - 2|A_0|^2B_0 = 0. \tag{6}$$

Although the nontrivial stationary solution $A_0(x)\neq 0$, $B_0(x)\neq 0$ cannot be obtained in closed form, its properties have been extensively studied [4,5].

The complex amplitudes A or B are next expanded in Fourier series as

$$A(x,y,z,t) = A_0(x) + \sum_{q_y,q_z} \hat{A}(q_y,q_z,x,t)e^{i(q_yy+q_zz)}, \tag{7}$$

$$B(x,y,z,t) = B_0(x) + \sum_{q_y,q_z} \hat{B}(q_y,q_z,x,t)e^{i(q_yy+q_zz)}. \tag{8}$$

By substituting Eqs. (7) and (8) into Eqs. (3) and (4), and linearizing the resulting equations in the perturbation amplitudes $\hat{A}$ and $\hat{B}$, we find

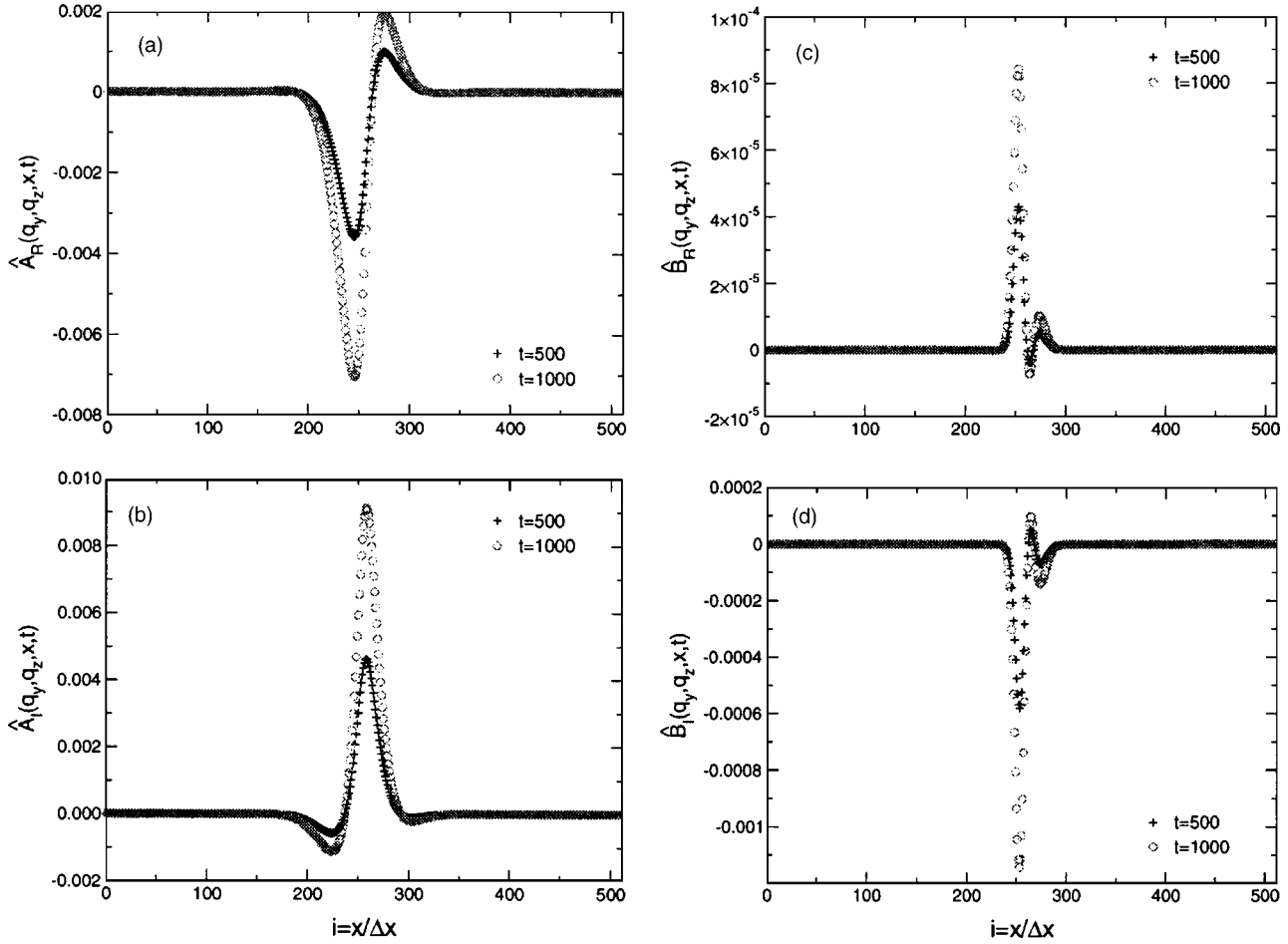

FIG. 2. (Color online) Perturbation amplitudes $\hat{A}$ and $\hat{B}$ as a function of grid index i along the x direction, for wave numbers $q_y=47/128$ and $q_z=5/64$, and $L_x=1024$, $\epsilon=0.04$, and initial noise amplitude 0.05. Both real ($\hat{A}_R$ and $\hat{B}_R$) and imaginary ($\hat{A}_I$ and $\hat{B}_I$) parts are shown at times $t=500$ (pluses) and 1000 (circles).

$$\partial_t \hat{A}(q_y,q_z,x,t) = [\epsilon - (2iq_0\partial_x - q_y^2 - q_z^2)^2 - 2|A_0|^2 - 2|B_0|^2]\hat{A}(q_y,q_z,x,t) - A_0^2\hat{A}^*(-q_y,-q_z,x,t) - 2A_0B_0^*\hat{B}(q_y,q_z,x,t) - 2A_0B_0\hat{B}^*(-q_y,-q_z,x,t), \quad (9)$$

$$\partial_t \hat{B}(q_y,q_z,x,t) = [\epsilon - (\partial_x^2 - q_y^2 - 2q_0q_z)^2 - 2|A_0|^2 - 2|B_0|^2]\hat{B}(q_y,q_z,x,t) - B_0^2\hat{B}^*(-q_y,-q_z,x,t) - 2A_0^*B_0\hat{A}(q_y,q_z,x,t) - 2A_0B_0\hat{A}^*(-q_y,-q_z,x,t), \quad (10)$$

where "$*$" denotes complex conjugation.

Since the solution to the base state equations (5) and (6) cannot be obtained analytically, we proceed as follows: We consider an initial configuration that has a pair of symmetric grain boundaries so that periodic boundary conditions can be used in a numerical solution. Planar grain boundaries on the yz plane are located at $x=L_x/4$ and $3L_x/4$, where L_x is the system size along the x direction. The two boundaries need to be sufficiently far apart from each other so that their motion is independent. We have verified that this is the case for the system sizes used in our study. We then numerically solve Eqs. (5) and (6), and use the result to solve Eqs. (9) and (10) for given, fixed values of q_y and q_z. A computational domain of size $L_x\times L_y\times L_z$ is divided into an evenly spaced grid, with eight grid points per wavelength of the base solution $\lambda_0=2\pi/q_0$. Hence the corresponding grid spacing is $\Delta x=\Delta y=\Delta z=\lambda_0/8$. We use a pseudospectral method with a Crank-Nicholson time stepping scheme for the linear terms, and a second order Adams-Bashford explicit algorithm for the nonlinear terms. A relatively large time step Δt can be used while maintaining stability; $\Delta t=0.2$ has been used in all of our calculations.

The stability of the base planar boundary is carried out indirectly by introducing small random perturbations into $\hat{A}$ and $\hat{B}$, with both real and imaginary parts, and solving the initial value problem defined by Eqs. (9) and (10). If the planar grain boundary is stable, the perturbations $\hat{A}$ and $\hat{B}$ would decay in time for all wave numbers (q_y,q_z). However, our calculations show there exists a range of (q_y,q_z) within which perturbations grow with time, indicating instability.

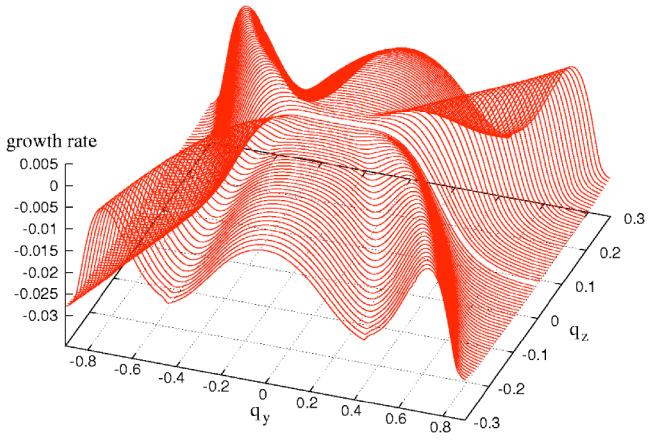

FIG. 3. (Color online) Perturbation growth rate σ as a function of wave numbers q_y and q_z, with the same values of the parameters ϵ, L_x, and the initial noise amplitude as those of Fig. 2. The maximum growth rate is found to be 1.35×10^{-3}, corresponding to four symmetric wave-number positions $(\pm q_y^{\max}, \pm q_z^{\max})$, with $q_y^{\max}=47/128$ and $q_z^{\max}=5/64$.

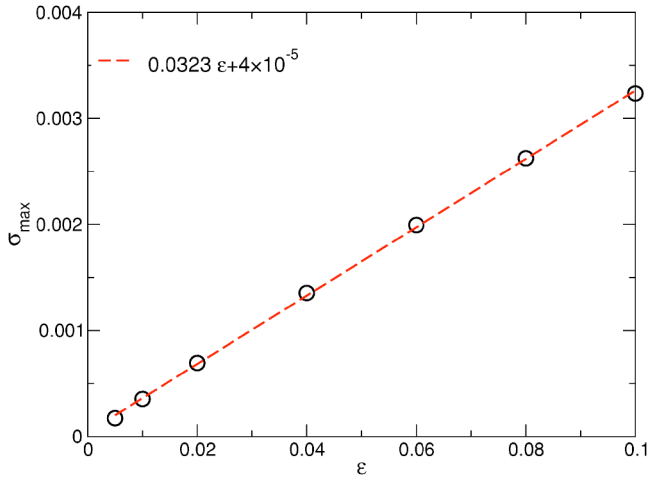

FIG. 4. (Color online) Maximum perturbation growth rate as a function of ϵ, with system size $L_x=1024$. The dashed line is a linear fit to the data yielding a slope of 0.0323 ± 0.0003, and an intercept $(4\pm1)\times10^{-5}$.

A typical result within the unstable region of wave numbers is shown in Fig. 2. We consider $L_x=1024$ and $\epsilon=0.04$. A random initial condition for the fields $\hat{A}$ and $\hat{B}$ has been considered, of zero average and uniformly distributed in $(-0.05,0.05)$. Far from the boundary region, the perturbations in $\hat{A}$ and $\hat{B}$ are seen to decay as a function of time, an observation which is consistent with the fact that both bulk regions are in the stable region of the model's stability diagram. On the contrary, both real and imaginary parts of the perturbations near the boundary grow in time for the example chosen here ($q_y=47/128$ and $q_z=5/64$). The growth of the perturbation can be quantified by writing $\hat{A}=|\hat{A}|e^{i\phi_A}$ and $\hat{B}=|\hat{B}|e^{i\phi_B}$, and as expected we find that $|\hat{A}|$, $|\hat{B}|\propto e^{\sigma t}$ with $\sigma=\sigma(q_y,q_z)$ the perturbation growth rate. We also note that the phase perturbation for A becomes linear in space in the unstable region: $\phi_A\propto-\delta qx$, whereas ϕ_B remains uniform.

We have repeated this process for a range of perturbation wave numbers q_y and q_z and computed the growth rate σ. Our results are shown in Fig. 3 for $\epsilon=0.04$. We observe four unstable regions, with maxima of the growth rate $\sigma^{\max}$ located at $(\pm q_y^{\max}, \pm q_z^{\max})$. As further shown in Fig. 4, $\sigma_{\max}>0$ for $\epsilon>0$, and linearly increases with ϵ. The characteristic wave numbers for instability correspond to $q_y^{\max}$ and $q_z^{\max}$, and are plotted in Fig. 5 as filled circles $(q_y^{\max})$ and squares $(q_z^{\max})$. The figure also shows the results of a direct numerical solution of the Swift-Hohenberg equation (1) (pluses and stars in Fig. 5), which we discuss below. Although it is difficult to be certain about the limiting behavior as $\epsilon\to0$ (the development of the instability is very slow and the numerical results not very accurate), it appears from both Figs. 4 and 5 that $\sigma^{\max}$, $q_y^{\max}$, and $q_z^{\max}$ tend to zero in that limit.

Further insight into the instability can be gained by direct numerical solution of Eq. (1). The equation has been discretized on a evenly spaced grid of 256^3 nodes, and integrated with the same method described above. A typical configuration following the boundary instability is shown in Fig. 1. In this example, $\epsilon=0.08$, and an initial configuration comprising two planar and symmetric grain boundaries of wave number q_0 has been perturbed by a random field, uniformly distributed between $(-0.05,0.05)$. In this case we show in gray scale the value of the field ψ at $t=2500$. The instability manifests itself by finite wave-number undulations of the grain boundary along both spatial directions, a perturbation that is of course precluded in two dimensions.

We have determined the characteristic wavelengths of the instability from the power spectrum of the order parameter ψ. Figure 6 shows the structure factors $|\psi_{q_y}|$ (circles) and $|\psi_{q_z}|$ (squares), defined respectively as the one-dimensional Fourier transform of ψ on the boundary plane $x=L_x/4$ at

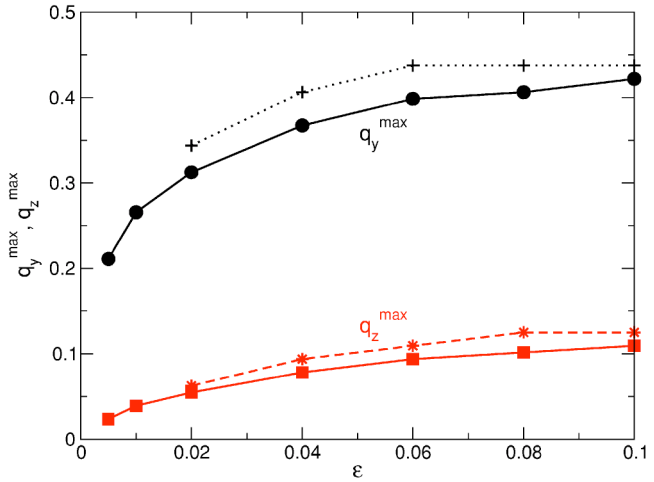

FIG. 5. (Color online) Characteristic wave numbers of instability $q_y^{\max}$ and $q_z^{\max}$ along two orthogonal directions of the grain boundary as a function of ϵ. Symbols (+ and $*$) correspond to results obtained from direct numerical solution of the model equation (1) with system size 256^3, while filled circles and squares with solid lines have been determined from the stability analysis of the amplitude equations (3) and (4) with $L_x=1024$.

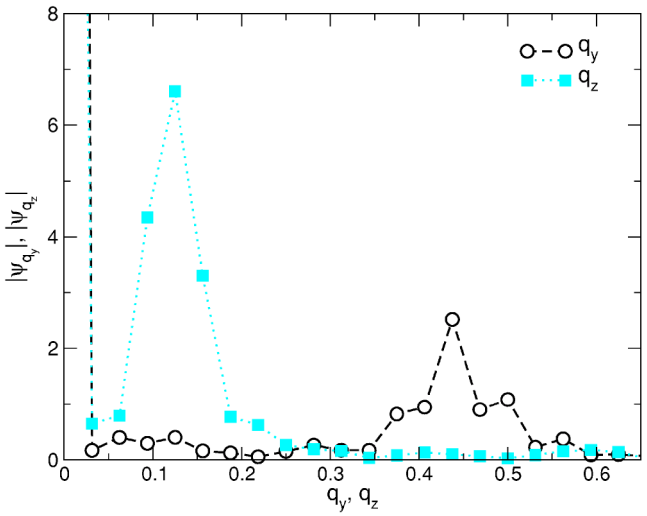

FIG. 6. (Color online) One-dimensional structure factor $|\psi_{q_y}|$ (at $z=L_z/2$) or $|\psi_{q_z}|$ (at $y=L_y/2$) on the grain boundary plane $x=L_x/4$ as a function of wave number q_y or q_z, respectively. The parameters are the same as those of Fig. 1, except for $t=1650$.

fixed $z=L_z/2$, or fixed $y=L_y/2$. Both power spectra exhibit peaks at nonzero wave numbers along their respective direction. In the case shown in the figure, $q_y^{\max}=0.4375$ and $q_z^{\max}=0.125$, so that $q_z^{\max}<q_y^{\max}<q_0=1$. This result holds for the entire range of ϵ that we have studied, and agrees with the result of the stability analysis shown in Fig. 5. Note also that the wave numbers of maximum growth as determined from the power spectrum of ψ agree well with the values of $q_y^{\max}$ and $q_z^{\max}$ obtained from the stability analysis.

III. CROSS ROLL INTERACTION IN THREE DIMENSIONS

It may appear somewhat surprising that, given that the planar grain boundary configuration is uniform in the y direction, and that the boundary is stable against perturbations in the xz plane, it should be unstable in three dimensions as shown in Sec. II. The projection to a two-dimensional lamellar pattern on the xz plane is a 90° tilt grain boundary, which is known to be stable as long as both lamellar regions have a wave number equal to q_0 [1,2,4–6]. On the other hand, a two-dimensional projection on the xy plane involves coexistence of a region of lamellae A with a uniform region B with constant value of ψ (Fig. 1). This two-dimensional projection is clearly unstable, and boundary motion (from stable A to unstable B) would occur driven by free energy reduction. However, any such free energy difference between regions A and B is absent in three dimensions, and therefore the origin of the instability deserves further scrutiny.

We begin the analysis by assuming the following approximate functional dependence of the amplitudes A and B in a two-dimensional system [15]:

$$A(x,z,t) \simeq A_0(x - X(z,t)), \quad B(x,z,t) \simeq B_0(x - X(z,t)), \tag{11}$$

under weak local distortion $X(z,t)$ of the grain boundary [A_0 and B_0 are the stationary solutions given by Eqs. (5) and (6)]. An equation of motion for the interface can be derived by substituting Eqs. (11) into the amplitude equations (3) and (4) (without the terms involving ∂_y^2), and expanding to first order in X. By using $X(z,t)=\Sigma_{q_z}\hat{X}_q(t)e^{iq_z z}$, we find that $\hat{X}_q(t)=\hat{X}_q(0)e^{\sigma_X(q_z)t}$, with σ_X the growth rate of the perturbation in X given by

$$\begin{aligned}\sigma_X(q_z) = &- \frac{1}{\int_{-\infty}^{\infty} dx(|\partial_x A_0|^2 + |\partial_x B_0|^2)} \\ &\times \int_{-\infty}^{\infty} dx[|\partial_x A_0|^2(-\epsilon + |A_0|^2 + 2|B_0|^2 + q_z^4) \\ &+ |\partial_x B_0|^2(-\epsilon + 2|A_0|^2 + |B_0|^2 + 4q_0^2 q_z^2) + 4q_0^2|\partial_x^2 A_0|^2 \\ &+ |\partial_x^3 B_0|^2 + (\partial_x|A_0|^2)^2/2 + (\partial_x|B_0|^2)^2/2 \\ &+ 2(\partial_x|A_0|^2)(\partial_x|B_0|^2)].\end{aligned} \tag{12}$$

We note from Eq. (12) both that $\sigma_X(q_z=0)=0$, and that σ_X decreases monotonically with q_z^2. Therefore $\sigma_X<0$ for all nonzero q_z. Within this approximation, a perturbed grain boundary always relaxes to the stationary planar state, as is already well known.

Consider next the analog of Eq. (11) for a three-dimensional system,

$$A(x,y,z,t) \simeq A_0(x - X(y,z,t)),$$

$$B(x,y,z,t) \simeq B_0(x - X(y,z,t)). \tag{13}$$

The resulting interfacial equation to first order in X is similar to Eq. (12), with some extra terms proportional to q_y^2 and q_y^4. It is easy to show that the same results follows, namely $\sigma_X(q_y,q_z)<0$ for all (q_y,q_z), i.e., a stable grain boundary, contrary to the calculations shown in Sec. II.

The inconsistency in the three-dimensional results can be traced back to the fact that assumption (11) does not allow for an imaginary part of A or B because the stationary solutions A_0 and B_0 are both real. Therefore no phase winding is allowed, a result which is consistent with wave-number selection in two dimensions, but that does not seem to be observed in three dimensions [cf. Figs. 2(b) and 2(d)]. We therefore argue that growth of phase perturbations is one of the major causes of the instability in three dimensions.

In order to illustrate how combined phase and amplitude modulations around the grain boundary can lead to a decrease in free energy, we recall that the amplitude equations (3) and (4) can be written in gradient form

$$\partial_t A = -\delta\mathcal{F}/\delta A^*, \quad \partial_t B = -\delta\mathcal{F}/\delta B^*,$$

with a potential $\mathcal{F}$

$$\begin{aligned}\mathcal{F} = \int\int\int dxdydz[&-\epsilon(|A|^2 + |B|^2) + (|A|^4 + |B|^4)/2 \\ &+ 2|A|^2|B|^2 + |(2iq_0\partial_x + \partial_y^2 + \partial_z^2)A|^2 \\ &+ |(\partial_x^2 + \partial_y^2 + 2iq_0\partial_z)B|^2].\end{aligned} \tag{14}$$

The net change $\Delta\mathcal{F}$ relative to the planar grain boundary is

$$\Delta\mathcal{F} = \mathcal{F} - \mathcal{F}_0, \tag{15}$$

where $\mathcal{F}_0$ of the base state is obtained by replacing A and B in Eq. (14) with the stationary solutions $A_0(x)$ and $B_0(x)$. By using the Fourier expansions (7) and (8), we have calculated $\Delta\mathcal{F}$ up to second order in the perturbations $\hat{A},\hat{B}$: $\Delta\mathcal{F} = \Delta\mathcal{F}^{(1)} + \Delta\mathcal{F}^{(2)}$. The first order result for $\Delta\mathcal{F}^{(1)}$ is

$$\begin{aligned}\Delta\mathcal{F}^{(1)} = V_{yz}\int dx\{&2(-\epsilon + |A_0|^2 + 2|B_0|^2)\mathrm{Re}[A_0\hat{A}^*(0)] \\ &+ 2(-\epsilon + 2|A_0|^2 + |B_0|^2)\mathrm{Re}[B_0\hat{B}^*(0)] \\ &+ 8q_0^2\,\mathrm{Re}[\partial_x A_0\partial_x\hat{A}^*(0)] + 2\mathrm{Re}[\partial_x^2 B_0\partial_x^2\hat{B}^*(0)]\},\end{aligned} \tag{16}$$

with $V_{yz} = L_y \times L_z$, $\hat{A}(0) = \hat{A}(q_y = q_z = 0, x, t)$, and $\hat{B}(0) = \hat{B}(q_y = q_z = 0, x, t)$. Given the numerical solution for the amplitudes of the perturbation described in Sec. II, we find that $\Delta\mathcal{F}^{(1)}$ is negligible (except for an initial transient related the fast local relaxation of the configuration in response to the random field which is added to the initial configuration). Therefore $\Delta\mathcal{F}$ is mostly determined by the second order result,

$$\begin{aligned}\Delta\mathcal{F}^{(2)} = V_{yz}\int dx \sum_{q_y,q_z}\Big\{&(-\epsilon + |A_0|^2 + 2|B_0|^2)|\hat{A}(\mathbf{q})|^2 + (-\epsilon \\ &+ 2|A_0|^2 + |B_0|^2)|\hat{B}(\mathbf{q})|^2 + |(2iq_0\partial_x - q_y^2 - q_z^2)\hat{A}(\mathbf{q})|^2 \\ &+ |(\partial_x^2 - q_y^2 - 2q_0q_z)\hat{B}(\mathbf{q})|^2 + \tfrac{1}{2}[|A_0^*\hat{A}(\mathbf{q}) + A_0\hat{A}^*(-\mathbf{q})|^2 \\ &+ |B_0^*\hat{B}(-\mathbf{q}) + B_0\hat{B}^*(\mathbf{q})|^2] + 2[A_0^*\hat{A}(\mathbf{q}) + A_0\hat{A}^*(-\mathbf{q})] \\ &\times[B_0^*\hat{B}(-\mathbf{q}) + B_0\hat{B}^*(\mathbf{q})]\Big\},\end{aligned} \tag{17}$$

with $\hat{A}(\mathbf{q}) = \hat{A}(q_y, q_z, x, t)$, and $\hat{B}(\mathbf{q}) = \hat{B}(q_y, q_z, x, t)$. $\Delta\mathcal{F} < 0$ indicates instability against the perturbation, while $\Delta\mathcal{F} > 0$ refers to the energy penalty of any modulations with the system relaxing to its stationary base state.

We now estimate $\Delta\mathcal{F}$ in both two and three dimensions by approximating the sums in Eq. (17) by the values at $(\pm q_y^{\max}, \pm q_z^{\max})$, the wave numbers associated with the largest growth rate $\sigma_{\max}$, and present the results in Fig. 7. In two dimensions, $\Delta\mathcal{F}$ [given by Eq. (17) with $q_y = 0$] remains positive for all times as expected (solid line). There is a negative contribution to $\Delta\mathcal{F}$ arising from the last term of Eq. (17) which reflects the coupling between A and B modes [dot-dashed line in Fig. 7(a)]. This term only contributes to the energy integral in the boundary region, and is negligible otherwise. However, the remaining positive contributions to Eq. (17) dominate (dashed line in the figure), leading to the overall stability of the boundary. On the other hand, the cross mode coupling in three dimensions dominates over the remaining stabilizing terms, leading to overall instability, as shown in Fig. 7(b). It is therefore the additional phase space available for the coupling between A and B modes at the boundary that is responsible for the instability in three dimensions.

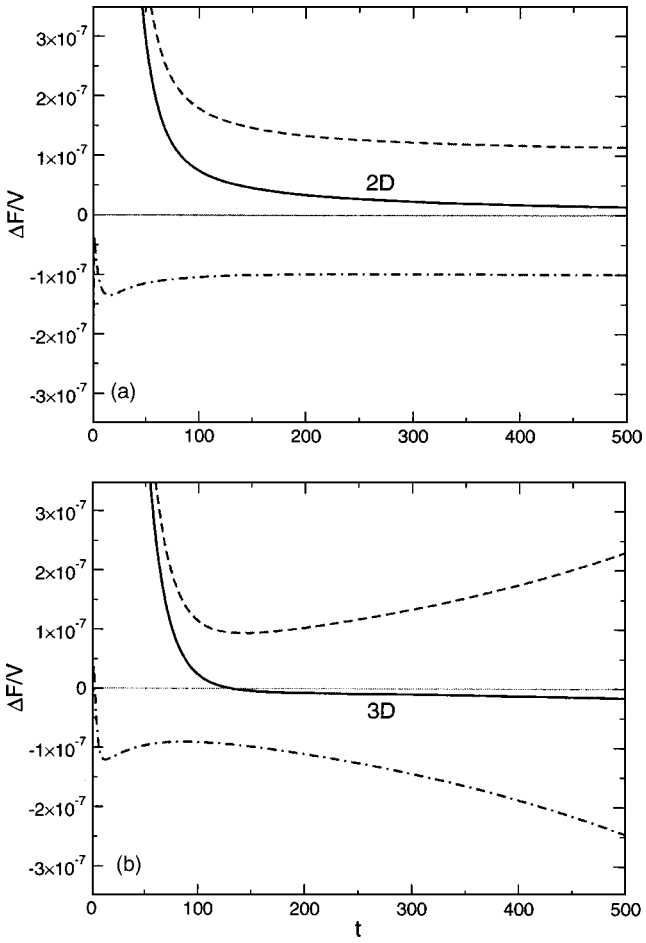

FIG. 7. (Color online) Time evolution of effective free energy density (per unit volume $V = L_x \times L_z$ or $V = L_x \times L_y \times L_z$) of the perturbed state, for (a) two- and (b) three-dimensional systems. In both (a) and (b), the net energy change $\Delta\mathcal{F}$ (thick solid curve) is the combination of the negative contribution from the last term of Eq. (17) (dash dotted curve) and all the remaining (positive) terms (dashed curve). The parameters used here are the same as in Fig. 2, except that in the two-dimensional system $|q_z| = 1/128$ has been used in the calculation.

IV. DISCUSSION AND CONCLUSIONS

We have found a finite wave-number instability associated with a 90° tilt grain boundary in a three-dimensional lamellar phase, both from direct numerical solution of the Swift-Hohenberg model equation, and an analysis of the corresponding amplitude equation. The latter result is therefore more generic and applies to grain boundaries in phases of smectic symmetry. The mode of instability is anisotropic on the grain boundary plane, with wavelengths along both directions that are larger than the wavelength of the base lamellar pattern. Of the two, the larger wavelength is directed along the normal to the lamellae oriented normal to the boundary plane. Both the characteristic wave numbers of the instability and the growth rate increase with ϵ.

The instability is accompanied by phase perturbation, a mode that is absent in two dimensions, and that results from the cross coupling of the two lamellar modes in the boundary

region. This coupling is also present in two dimensions, but it is not strong enough to produce instability.

It is important to verify that this instability is not an artifact of finite size effects inherent to all our calculations. It is known, for example, that there is net boundary attraction when their separation is not much larger than their width, the latter scaling as $\epsilon^{-1/2}$ for small ϵ [4]. Our system sizes have been chosen large enough so that the pair of grain boundaries in the computational domain remain stationary in a two-dimensional geometry. Spot checks of the results shown in Figs. 1, 5, and 6, with different system sizes have revealed no discernible change.

The instability described above is different from that which is caused by deviations of the base lamellar wave number q_x (in region A) or q_z (in region B) from q_0 [4,5]. Such an instability is also present in three dimensions. We have studied grain boundary configurations in three dimensions with different values of $q_x = q_z = q_0 + \Delta q$, with Δq small. Our calculations show that the boundaries move toward each other (from region A to B) as long as $\Delta q \neq 0$. The wave number q_x of lamellae A always relaxes to the optimum value $q_0 = 1$, leading to the creation of new lamellae for $\Delta q > 0$ (with Δq small enough to remain inside the stability region of lamellar phase [11]), or to the disappearance of existing lamellae for $\Delta q < 0$, similar to the two-dimensional results of Ref. [5]. During the process, the wave number q_z of lamellae B remains constant, with the extent of region B decreasing with time due to the invasion by lamellae A. In the case of $\Delta q < 0$, lamellae B also undergo a zigzag instability.

In experiments of three-dimensional lamellar diblock copolymers, 90° tilt boundaries (the configuration studied here: Fig. 1) have been observed, but with very low frequency compared to other types of tilt grain boundaries [12]. This observation is consistent with the three-dimensional instability obtained above, although the instability itself has not been directly observed. It would be interesting to reexamine the experimental images to determine the possible existence of lamellar undulations in the vicinity of grain boundaries, and measure the wavelengths of such modulations. The decay of the 90° tilt boundary is very slow for small ϵ, and could manifest itself in undulations at boundaries.

In summary, our results indicate that 90° tilt grain boundaries should be rare in three-dimensional extended samples, but readily observable in two-dimensional systems. This is in agreement with experimental findings in three-dimensional lamellar phases [12], and with numerical evidence in the case of two dimensions [1,2]. Following the boundary instability in three dimensions, we observe growth and a limited amount of coarsening near the boundary region. However, the evolution is very slow, and we cannot determine whether a stationary state will be reached, or whether evolution will continue until the two boundaries annihilate each other.

ACKNOWLEDGMENTS

This research has been supported by the National Science Foundation under Grant No. DMR-0100903 and by NSERC Canada.

[1] M. C. Cross and P. C. Hohenberg, Rev. Mod. Phys. **65**, 851 (1993).
[2] P. Manneville, *Dissipative Structures and Weak Turbulence* (Academic, New York, 1990).
[3] G. H. Fredrickson and F. S. Bates, Annu. Rev. Mater. Sci. **26**, 501 (1996).
[4] P. Manneville and Y. Pomeau, Philos. Mag. A **48**, 607 (1983).
[5] G. Tesauro and M. C. Cross, Philos. Mag. A **56**, 703 (1987).
[6] B. A. Malomed, A. A. Nepomnyashchy, and M. I. Tribelsky, Phys. Rev. A **42**, 7244 (1990).
[7] D. Boyer and J. Viñals, Phys. Rev. E **64**, 050101 (2001).
[8] Z.-F. Huang, F. Drolet, and J. Viñals, Macromolecules **36**, 9622 (2003).
[9] Z.-F. Huang and J. Viñals, Phys. Rev. E **69**, 041504 (2004).
[10] F. H. Busse, Rep. Prog. Phys. **41**, 1929 (1978).
[11] H. S. Greenside and W. M. Coughran, Jr., Phys. Rev. A **30**, 398 (1984).
[12] S. P. Gido and E. L. Thomas, Macromolecules **27**, 6137 (1994).
[13] J. Swift and P. C. Hohenberg, Phys. Rev. A **15**, 319 (1977).
[14] G. H. Fredrickson, J. Rheol. **38**, 1045 (1994).
[15] We are indebted to David Jasnow for discussions about interfacial equations of motion.